

PROCESS-SPECIFIC MICROSTRUCTURE-SENSITIVE MODELING OF FATIGUE IN ADDITIVELY MANUFACTURED TI-6AL-4V ALLOYS

Lionardo Lado^a, Saeed Ataollahi^a, Aref Yadollahi^b, and Mohammad J. Mahtabi^{a,*}

^a Department of Mechanical Engineering, The University of Tennessee at Chattanooga,
Chattanooga, TN, 37403

^b William B. Burnsed, Jr. Department of Mechanical, Aerospace, and Biomedical Engineering,
University of South Alabama, Mobile, AL, 36688, USA

*Corresponding author: Mohammad-Mahtabi@utc.edu

Abstract

Thanks to its high strength-to-weight ratio and corrosion resistance, Ti-6Al-4V has gained a lot of attention in additive manufacturing (AM) of complex parts with aerospace and medical applications. The realistic loading condition in these applications is mostly cyclic, thus fatigue failure is the main mode of failure. On the other hand, due to presence of local defects in the current state of AM materials, the main challenge with AM of metallic parts is their fatigue resistance and durability, being much lower than the conventional counterparts. In this study, a simplified microstructure-sensitive fatigue (MSF) approach was developed to model the fatigue life of AM Ti-6Al-4V specimens by incorporating microstructural features and defect properties, such as grain size, pore size and pores nearest neighbors. The studied AM methods include Laser Engineered Net Shaping (LENS), Electron Beam Melting (EBM), and Selective Laser Melting (SLM). Each of these processes use different approaches in constructing the three-dimensional object, yielding in different microstructure of the final part. For this work, microstructural data were collected from previous experimental studies. Scanning Electron Microscopy (SEM) images were used to examine the fracture surfaces of the AM specimens and determine the defects responsible for fatigue failure. With an emphasis on the microstructurally small crack growth, model parameters were calibrated for fatigue data for different AM processes, while keeping process-independent parameters as constant. The results showed that a simplified MSD fatigue model with limited number of process-dependent governing parameters can be calibrated for each set of data.

Keywords: Microstructure-sensitive fatigue, Additive manufacturing, Ti-6Al-4V, EBM, LENS, SLM

1- Introduction

Additive manufacturing (AM) has shown a great potential in minimization of material waste and lowering the fabrication cost and labor of complex parts. AM allows for the creation of customized three-dimensional items for engineering applications. A significant amount of attention has been paid to this advanced manufacturing process in various industries, especially to fabricate metallic parts. At the current state of AM, monotonic mechanical properties as good as those for wrought material can be obtained for AM parts [1, 2]. However, among the various

mechanical properties, fatigue is the most sensitive one to the AM process parameters due to the local nature of the fatigue and presence of local defects in the AM part. As a result, the fatigue resistance of AM materials is generally inferior to their wrought counterparts. The short fatigue life of AM parts is the main obstacle towards employing AM for engineering applications. It should be mentioned that although post processing methods like heat treatment [3] and hot isostatic pressing (HIP) [4, 5] may reduce the number of defects and improve the fatigue resistance of AM parts, they have some undesired effects such as reducing the part accuracy and change in microstructure among others. Moreover, post-processing reduces the cost-effectiveness of AM and, nevertheless, the ultimate goal of AM is to fabricate ready-to-service parts.

Due to the large number of process parameters — such as laser power, scanning speed, layer thickness, hatch spacing, etc. — the microstructure of the final product, thus its mechanical properties and fatigue resistance, varies significantly by alteration of each of the process parameters, even when using the same AM method. Therefore, there has been a significant research effort in the past decade to study the fatigue behavior of AM alloys, to determine the causes of fatigue failure, and to develop predictive models to estimate the fatigue life of these components [4, 6-9].

Employing predictive methods to study the fatigue behavior of additively manufactured materials will provide a better understanding on how each AM processing parameter affects the fatigue resistance of the fabricated part. Such an understanding can be used to tune the process parameters to tailor the desired fatigue resistance of the AM parts. In this regard, microstructure-sensitive fatigue models can bridge the process-structure-property relation by linking the fatigue properties to the microstructure of the material, and further to the processing parameters. Microstructure-sensitive fatigue (MSF) model is a microstructure-sensitive fatigue model which originally was developed for fatigue life prediction of cast aluminum alloys [10]. It can explicitly incorporate the effect of different microstructural features and defects into the prediction of fatigue life. MSF has also been calibrated to predict fatigue behavior of several wrought materials [6, 11, 12].

Among metal alloys, titanium alloys have a considerable share in the AM market. Ti-6Al-4V alloy possesses unique engineering properties, such as a good combination of high strength, toughness, corrosion resistance, ductility, and biocompatibility [13, 14]. These characteristics have made Ti-6Al-4V a popular candidate for various applications in the medical and aerospace industries [15, 16]. Therefore, in this study, the microstructure-sensitive fatigue modelling of this alloy was considered. The model that was first calibrated for the conventional material and then used, by adjusting only a limited number of inherently process-dependent parameters, to predict and compare the fatigue behavior of the same alloy fabricated by different AM methods.

2- Materials and Method

2-1- Experimental data

Fatigue data for different AM methods including Laser Engineered Net Shaping (LENS), Electron Beam Melting (EBM), and Selective Laser Melting (SLM) were used to develop MSF models in this study. The microstructural data corresponding to specimens of each fabrication

method were obtained from the scanning electron microscopy images of the fatigue specimens. These data were used in the MSF model to generate strain-controlled fatigue curves for each set of input data, corresponding to each of the AM methods. Even though the material was the same in the different sets of data, the microstructural characteristics were different due to the differences in the fabrication method. These microstructural features include grain size and orientation as well as defects properties, such as pore size and spacing.

Laser Engineered Net Shaping (LENS) fabricated Ti-6Al-4V specimens have shown to have a unique microstructural feature in which the grains have a distinguished shape. When examined, the β grains were columnar and there were fine α morphologies. Depending on the power input, high magnification imaging of the microstructure indicates a martensite microstructure with acicular α or mix of α - β lamellae [15]. This is determined to be a result of multiple factors such as the cyclic heating, directional heat extraction and the fast-cooling rate [15]. EBM samples demonstrate a similar morphology to LENS in that their β grains are columnar. However, during the fabrication process the specimens were relatively slowly cooled, unlike LENS samples which experience a fast cooling [15]. Thus, the microstructure had an α - β lamellae at high magnification [15]. Since EBM is a powder bed fusion technique, it will have two types of pores that can form during the built process. The first type is gas pore that is caused by trapped gas in the specimen and is spherical, while the other type is un-melted regions caused by insufficient melting. In addition, because of the lack of the martensite phase, the ductility of the EBM specimen is higher than that of the LENS [15]. Selective Laser Melting (SLM) exhibits similar microstructural morphologies to the other additive manufacturing methods. This is demonstrated by the columnar β grains, with acicular α martensite [17]. This will give the material a higher tensile strength, but it will suffer from lower ductility as proven also in the LENS specimens. Improving the ductility of the specimen to have α - β lamellae can only be done by using heat treatment or cyclic reheating during the build process [17].

The data for different sets of fatigue experiments were collected from the literature for conventional [18], EBM [19], LENS [20], and SLM [21] Ti-6Al-4V alloy. Three types of data were needed for calibration of MSF model: (1) strain-life fatigue data, (2) microstructural features and defects, and (3) mechanical properties. All the data were selected for the same strain ratio of $R = -1$. To consider the variations only due to fabrication methods, the data were chosen for the as-built specimens without any post-fabrication treatment. Moreover, the required mechanical and microstructural data for each set of data were collected from the micrographs provided in the corresponding reference using ImageJ [22] image processing software. Figure 1 shows the experimental strain-life fatigue data for the different sets of data used in this study. In addition, Figure 2 shows an example of a void in a Ti-6Al-4V specimen fabricated by LENS methods [20], which was quantified in this study. Finally, Table 1 presents a summary of the compiled microstructural data used for MSF modeling that were obtained from the references. In this table, pore nearest neighbor distance (PORENND) implies the proximity of pores in a specimen.

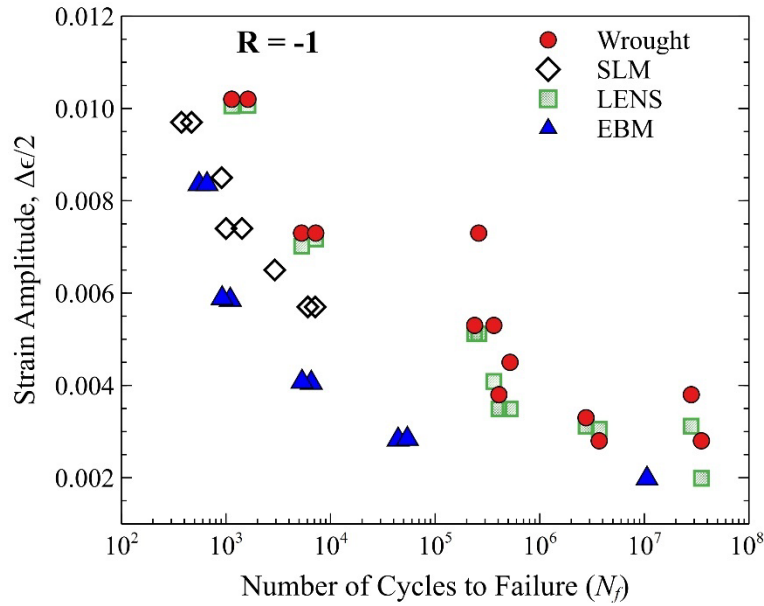


Figure 1- Experimental strain-based fatigue data [18-21] used for calibration of the MSF model.

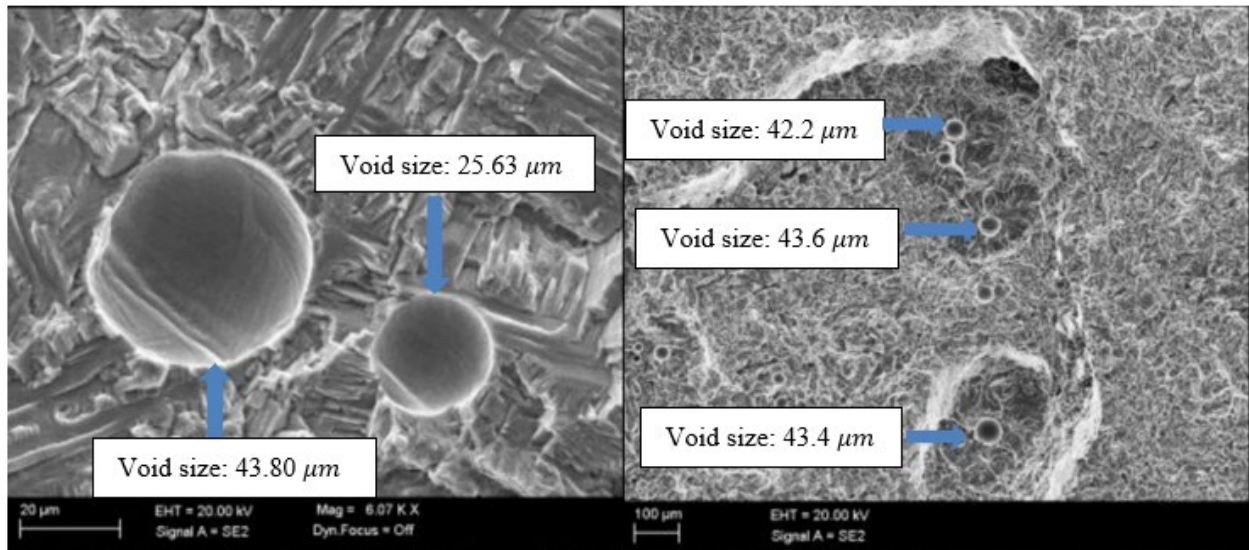


Figure 2- An example of defect in Ti-6Al-4V samples fabricated using LENS method [20]. These features were quantified for MSF model.

Table 1- Measured microstructural input parameters needed for the microstructure-sensitive fatigue model of various Ti-6Al-4V specimens

Parameter	Conventional	EBM	LENS	SLM
Pore size (μm)	0.001	73	42.9	22
Pore NND (μm)	0.007	513	303.6	409.5
Grain size (μm)	5	4.7	320.4	2.89

2-2- The MSF model

The microstructure-sensitive, multistage fatigue (MSF) model used in this work was originally developed by McDowell et al. [10]. This model has shown successful application in modeling the fatigue of various metallic materials [6, 11, 12]. The MSF divides the fatigue life of a material into three stages. Crack incubation, which is the number of cycles to incubate a fatigue crack (N_{Inc}). Following this stage, the incubated crack, which is small relative to the microstructural features of the materials, will grow for a certain number of cycles (N_{MSC}). The third stage is the number of cycles that takes for a crack, which is now large relative to the microstructural features of the materials, to grow (N_{LC}), before the final failure. The total number of cycles to failure, N_{Total} , is then equal to [10]:

$$N_{Total} = N_{Inc} + N_{MSC} + N_{LC} \quad (1)$$

For the current state of AM materials, there are always unintentional defects present in the printed part that can act as existing cracks. In addition, the long-crack growth stage of fatigue has shown to be relatively independent of the AM method and in some cases similar to the wrought material [23]. Therefore, the incubation and long-crack growth stages of fatigue were excluded in this work and the focus was put on small-crack growth for modeling. In addition, this enables developing a simpler, yet realistic microstructure-sensitive fatigue model, specific to AM materials.

Crack growth rate in the microstructurally small-crack growth regime, $\left(\frac{da}{dN}\right)_{MSC}$, is driven by the range of crack-tip displacement (ΔCTD). Equation (2) [10], demonstrates this by multiplying a material constant, χ , crack growth rate constant (which represents the crack-tip irreversibility), by the difference of crack-tip displacement and the crack-tip displacement threshold (ΔCTD_{th}). The crack-tip displacement threshold is calculated based on the Burgers vector of the material, and thus depends on the crystal structure.

$$\left(\frac{da}{dN}\right)_{MSC} = \chi(\Delta CTD - \Delta CTD_{th}) \quad (2)$$

The crack-tip displacement range depends on various features of the microstructure, as presented in Equation (3) [10]. In this equation, C_I and C_{II} are low-cycle and high-cycle fatigue constants for small cracks, respectively. GS and GO represent the grain size and orientation for the material. GS_0 and GO_0 are the reference grain size and orientation, respectively. $\Delta\hat{\sigma}$ is the equivalent applied stress and U is considered as the load ratio parameter. This equation implies that the crack opening occurs in the tensile part of the cyclic load. Initial crack length is specified by “ a ” and macroscopic maximum plastic shear strain amplitude is denoted by $\left(\frac{\Delta\gamma_{max}^p}{2}\right)_{macro}$. The parameters that are material constants include C_I , C_{II} , ϖ , ξ , ϖ' , ξ' and ζ . Further details about the equations and parameters of the MSF can be found in the related references [24, 25].

$$\Delta CTD = C_{II} \left(\frac{GS}{GS_0}\right)^\varpi \left(\frac{GO}{GO_0}\right)^\xi \left[\left(\frac{U\Delta\hat{\sigma}}{S_{ut}}\right)^\zeta\right] a + C_I \left(\frac{GS}{GS_0}\right)^{\varpi'} \left(\frac{GO}{GO_0}\right)^{\xi'} \left(\frac{\Delta\gamma_{max}^p}{2}\right)_{macro}^2 \quad (3)$$

The values of the material constants that were process independent, thus were kept the same for each AM process, are listed in Table 2. For example, the crack tip displacement threshold value based on Burgers vector for titanium, was set to 3×10^{-9} [10]. Among all the “process-independent” parameters of the MSF, the only parameter that was changed for each AM process was the strain hardening exponent in the incubation stage [10]. This parameter was modified only when certain information was not available for the small crack growth stage. Cyclic strain hardening exponent from fatigue testing of each of the AM processes was extracted from the corresponding reference to modify the curve. Most often this parameter affects the slope of the MSF-based fatigue curve for the material. The parameters that were not material constants were then calibrated to fit the curve to the experimental data. The final values of the process-dependent parameters for each set of the fatigue data are reported in Table 3.

Table 2- Calibrated material constants for the microstructurally small crack for the MSF model for Ti-6Al-4V

Material Constant	Description	Value
C_I	Low cycle fatigue constant	10000
C_{II}	High cycle fatigue constant	2
ϖ	Pore effect coefficient	0.5
γ	Crack growth rate constant	0.32
ΔCTD_{th}	Crack Tip Displacement threshold	0.0003
CNC	Constant related to Coffin Manson	0.56
C_m	Ductility of coefficient in Coffin Manson	0.15
α	Ductility exponent of Coffin Manson law	-0.6
Y_1	Constant in remote strain to local strain to local plastic shear strain	200
Y_2	Linear in remote strain to local strain to local plastic shear strain	100
q	Exponent in remote strain to local strain to local plastic shear strain	2.1
θ	Load path dependent and loading combination parameter	0
r	Exponent in micromechanics study	0.14
Tn	Small crack growth exponent	3.6

Table 3– Calibrated values of process-dependent parameters in the microstructure-sensitive fatigue model of Ti-6Al-4V

Parameter	Conventional	EBM	LENS	SLM
POREEXP	0.05	1.6	0.5	0.901
a_f	30	10	5	1
GOEXP	0	0.4	0.5	0.7
DCSEXP	0	1	2.5	4

3- Results and Discussion

A comprehensive list of the parameters involved in the MSF model can be found in the related literature (for example, [12]). In this study, for the microstructure-sensitive fatigue model, four of the parameters in microstructurally small crack growth stage were identified as process dependent

and are listed in Table 3. The effect of pore size to local plastic strain (POREEXP) parameter accounts for how the size of the pore can influence the fatigue. This parameter had a noticeable effect for each additive manufacturing method, where it can greatly shift the final fatigue curve. Another parameter is the final crack size (a_f) which is the upper bound length of a microstructurally small crack, i.e. beyond this length the crack will be considered a long crack. This parameter was also considered in calibrating the model for each of the AM methods and to obtain the curve corresponding to the experimental data. The exponents for the grain size (DCSEXP) and grain orientation (GOEXP) were used to calibrate the fatigue curve as well.

Figure 3 presents the calibrated graphs of conventional specimens based on the parameters in Table 3. The fatigue curve was greatly influenced by the POREEXP, while the final crack size parameter, a_f , had a small effect on the low cycle fatigue regime of the curve. These parameters were the only ones calibrated in the microstructurally small crack stage to model the experimental fatigue data. Once the process-independent parameters were calibrated based on the data for conventional specimens, these parameters were kept constant for modeling the AM data. The calibrated EBM graph is shown in Figure 4(a). The change in POREEXP parameter in EBM resulted in a different behavior compared to the conventional case, as by increasing the value for this parameter, it decreased the number of cycles. EBM had a larger pore size and PORENND parameter compared to the conventional case. In addition, the a_f parameter mainly influenced the low cycle fatigue regime, whereas the GOEXP and DCSEXP (grain characteristics) mainly affected the high cycle regime of the curve.

For the LENS data shown in Figure 4(b), the low-cycle portion of the curve was not affected by the change in the final crack size value (a_f). However, increasing the value of POREEXP parameter increased the number of cycles corresponding to a strain amplitude and thus shifting the curve to the right. The same behavior was noticed for modeling the SLM data, where Figure 4(c) shows the calibrated MSF curve. The difference between EBM and LENS/SLM in this regard is that EBM has the largest pore size, while the other additive manufacturing methods have smaller pore sizes that are less than 50 μm in size, as can be seen in Table 1.

Similar to the curve for conventional data, for LENS and SLM methods the low cycle fatigue regime was not governed by the final crack size parameter (a_f), while in EBM, a_f affected the low cycle regime significantly. In addition, grain size exponent's effect on high cycle regime of SLM was more pronounced. It implies that grain size effects are more pronounced at the high cycle fatigue regime (i.e., smaller strain amplitudes) for SLM specimens, which had the finest average grain size.

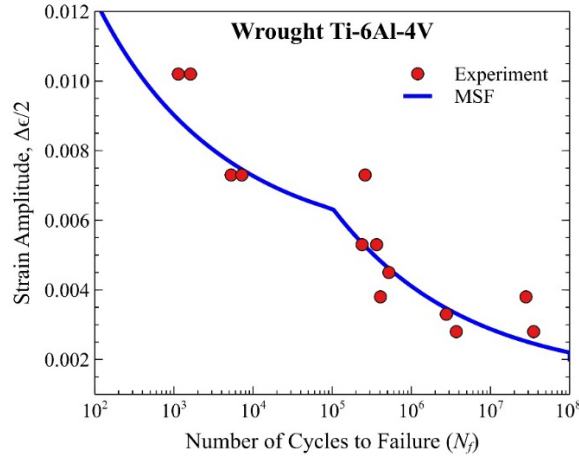


Figure 3- Calibrated fatigue curves using the microstructure-sensitive fatigue model for conventional Ti-6Al-4V data. All the process-independent parameters were used for the other sets of data.

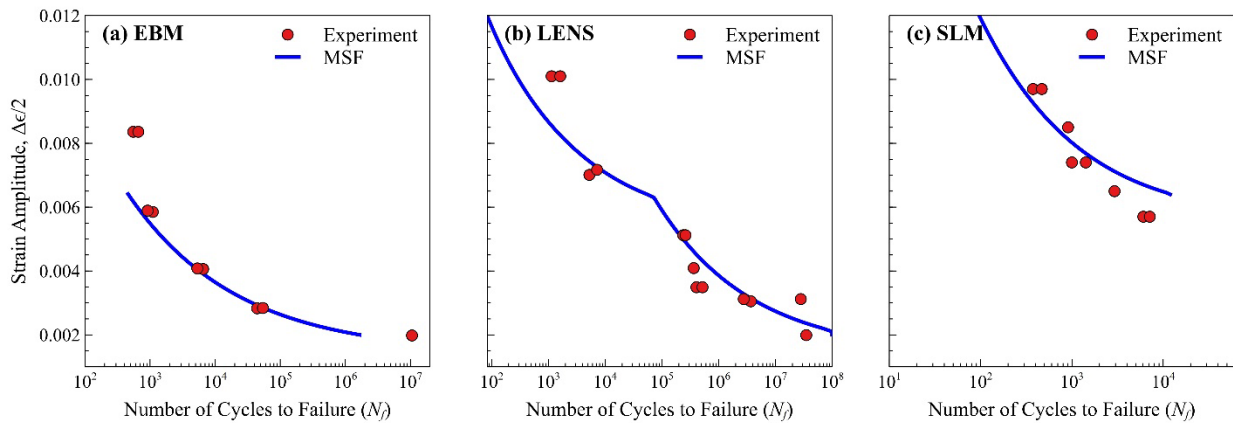


Figure 4- Calibrated fatigue curves using the microstructure-sensitive fatigue model for (a) as-built EBM, (b) as-built LENS, and (c) as-built SLM.

It is worth mentioning that MSF curves that more closely follow the experimental data could be generated by slightly modifying the rest of parameters. However, since the main intention of this work was to develop a simplified MSF model, the focus was only on the four process-dependent parameters.

Based on these results, by considering the small-crack growth data as the process-dependent parameters and keeping the rest of material parameters constant a simplified microstructure-sensitive fatigue model can be developed for additively manufactured metallic parts. In this regard, the fact that the current state of AM parts are not defect-free and various types of pores and unmelted regions are present that act as crack, can help simplifying the fatigue model by excluding the life for crack incubation. Furthermore, based on the observations that the long crack growth is a material property and is almost process independent, helps reducing the fatigue model to microstructurally small crack growth life and, thus, reducing the model parameters greatly.

For future works, more experimental data will be generated and collected from the literature to further tune the parameters of the model. In addition, since the parameters of the simplified MSF model depend on the process parameters, efforts will be made to establish the relations. As a

results, functions will be developed that can closely estimate the MSF parameters based on a given set of AM process parameters.

4- Conclusions

A microstructure-sensitive fatigue model was employed to study the fatigue behavior of AM Ti-6Al-4V fabricated using different additive manufacturing processes. By incorporating the material properties and the microstructural data extracted from SEM images, strain-life fatigue curves corresponding to each set of AM data was obtained using MSF model. The results of this work indicated a great potential for a simplified microstructure-sensitive fatigue model with limited number of process-dependent parameters. The parameters of the simplified model depend on the grain structure and defect characteristics, i.e., the pore size exponent, grain size exponent, final crack size, and grain orientation exponent in the MSF model. The simplified model can closely estimate the fatigue life of AM parts. As case study, in this work the fatigue life of Ti-6Al-4V specimens were closely estimated for conventional as well as LENS-, EBM- and SLM-fabricated specimens, only by altering the microstructure-related features and keeping the material-related parameters the same. The effects of pore size to local plastic strain parameter were the same for the LENS and SLM. Conversely, when increasing its value for EBM, that decreased the number of cycles. This behavior can be attributed to the larger pore size in EBM. For LENS and SLM data, final crack size did not have influence on low cycle fatigue regime while for EBM, it was a governing parameter in that region. The grain size exponent had significant influence on high cycle regime in SLM, indicating its fine grain size affects its fatigue resistance in small strain amplitudes.

References

1. Shamsaei, N., et al., *An overview of Direct Laser Deposition for additive manufacturing; Part II: Mechanical behavior, process parameter optimization and control*. Additive Manufacturing, 2015. **8**: p. 12-35.
2. Yadollahi, A., et al., *Fatigue behavior and failure analysis of additive manufactured inconel 718 superalloy*. Submitted for Publication to Materials Science and Engineering A, 2016.
3. Leuders, S., et al., *On the mechanical behaviour of titanium alloy TiAl6V4 manufactured by selective laser melting: Fatigue resistance and crack growth performance*. International Journal of Fatigue, 2013. **48**: p. 300-307.
4. Hrabe, N., T. Gnäupel-Herold, and T. Quinn, *Fatigue properties of a titanium alloy (Ti-6Al-4V) fabricated via electron beam melting (EBM): Effects of internal defects and residual stress*. International Journal of Fatigue, 2017. **94**: p. 202-210.
5. Qiu, C., N.J.E. Adkins, and M.M. Attallah, *Microstructure and tensile properties of selectively laser-melted and of HIPed laser-melted Ti-6Al-4V*. Materials Science and Engineering: A, 2013. **578**: p. 230-239.
6. Bagheri, A., et al., *Microstructure-Based MultiStage Fatigue Modeling of NiTi Alloy Fabricated via Direct Energy Deposition (DED)*. Journal of Materials Engineering and Performance, 2022. **31**(6): p. 4761-4775.
7. Bayati, P., et al., *Toward understanding the effect of remelting on the additively manufactured NiTi*. The International Journal of Advanced Manufacturing Technology, 2021. **112**(1): p. 347-360.

8. Yadollahi, A., et al., *Fatigue life prediction of additively manufactured material: Effects of surface roughness, defect size, and shape*. *Fatigue & Fracture of Engineering Materials & Structures*, 2018. **41**(7): p. 1602-1614.
9. Leuders, S., et al., *Fatigue Strength Prediction for Titanium Alloy TiAl6V4 Manufactured by Selective Laser Melting*. *Metallurgical and Materials Transactions A*, 2015. **46**: p. 3816-3823.
10. McDowell, D.L., et al., *Microstructure-based fatigue modeling of cast A356-T6 alloy*. *Engineering Fracture Mechanics*, 2003. **70**(1): p. 49-80.
11. Cagle, M.S., et al., *Characterization and modeling of the fatigue behavior of 304L stainless steel using the MultiStage Fatigue (MSF) Model*. *International Journal of Fatigue*, 2021. **151**: p. 106319.
12. Horstemeyer, M.F., et al., *Universal Material Constants for MultiStage Fatigue (MSF) Modeling of the Process–Structure–Property (PSP) Relations of A000, 2000, 5000, and 7000 Series Aluminum Alloys*. *Integrating Materials and Manufacturing Innovation*, 2020. **9**(2): p. 157-180.
13. Aboutaleb, A.M., et al., *Multi-objective accelerated process optimization of mechanical properties in laser-based additive manufacturing: Case study on Selective Laser Melting (SLM) Ti-6Al-4V*. *Journal of Manufacturing Processes*, 2019. **38**: p. 432-444.
14. Sidambe, A.T., *Biocompatibility of Advanced Manufactured Titanium Implants-A Review*. *Materials (Basel, Switzerland)*, 2014. **7**(12): p. 8168-8188.
15. Zhai, Y., H. Galarraga, and D.A. Lados, *Microstructure, static properties, and fatigue crack growth mechanisms in Ti-6Al-4V fabricated by additive manufacturing: LENS and EBM*. *Engineering Failure Analysis*, 2016. **69**: p. 3-14.
16. Niinomi, M., *Mechanical biocompatibilities of titanium alloys for biomedical applications*. *Journal of the Mechanical Behavior of Biomedical Materials*, 2008. **1**(1): p. 30-42.
17. Agius, D., K. Kourousis, and C. Wallbrink, *A Review of the As-Built SLM Ti-6Al-4V Mechanical Properties towards Achieving Fatigue Resistant Designs*. *Metals (Basel)*, 2018. **8**(1): p. 75.
18. Carrion, P.E., et al., *Fatigue behavior of Ti-6Al-4V ELI including mean stress effects*. *International Journal of Fatigue*, 2017. **99**: p. 87-100.
19. Zhang, Y., et al., *Multiple α sub-variants and anisotropic mechanical properties of an additively-manufactured Ti-6Al-4V alloy*. *Journal of Materials Science & Technology*, 2021. **70**: p. 113-124.
20. Sterling, A., et al., *Fatigue Behaviour of Additively Manufactured Ti-6Al-4V*. *Procedia Engineering*, 2015. **133**: p. 576-589.
21. Hu, D., et al., *Prediction of anisotropic LCF behavior for SLM Ti-6Al-4V considering the spatial orientation of defects*. *International Journal of Fatigue*, 2022. **158**: p. 106734.
22. Schneider, C.A., W.S. Rasband, and K.W. Eliceiri, *NIH Image to ImageJ: 25 years of image analysis*. *Nature Methods*, 2012. **9**(7): p. 671-675.
23. Yadollahi, A., et al., *Effects of crack orientation and heat treatment on fatigue-crack-growth behavior of AM 17-4 PH stainless steel*. *Engineering Fracture Mechanics*, 2020. **226**: p. 106874.
24. McDowell, D.L., et al., *Microstructure-based fatigue modeling of cast A356-T6 alloy*. *Engineering Fracture Mechanics*, 2003. **70**: p. 49-80.
25. Xue, Y., et al., *Microstructure-based multistage fatigue modeling of aluminum alloy 7075-T651*. *Engineering Fracture Mechanics*, 2007. **74**: p. 2810-2823.